

LETTER

Valence state partitioning of V between pyroxene and melt for martian melt compositions Y 980459 and QUE 94201: The effect of pyroxene composition and crystal structure

JAMES J. PAPIKE¹, PAUL V. BURGER^{1,*}, AARON S. BELL¹, CHARLES K. SHEARER¹, LOAN LE², JOHN JONES³ AND PAULA PROVENCIO¹

¹Institute of Meteoritics, Department of Earth and Planetary Sciences, University of New Mexico, Albuquerque, New Mexico 87131, U.S.A.

²JSC Engineering, Technology and Science (JETS), NASA Johnson Space Center, Houston, Texas 77058, U.S.A.

³NASA Johnson Space Center, Houston, Texas 77058, U.S.A.

ABSTRACT

A martian basalt (Yamato 980459) composition was used to synthesize olivine, spinel, and pyroxene at 1200 °C at five oxygen fugacities: IW-1, IW, IW+1, IW+2, and QFM. The goal of this study is to examine the significant variation in the value of $D_V^{\text{pyroxene/melt}}$ with changing Wo content in pyroxene. While most literature on this subject relies on electron microprobe data that assumes that if the Wo component (CaSiO₃) is <4 mol%, the pyroxene is in fact orthopyroxene, we've made a more robust identification of orthopyroxene using appropriate Kikuchi diffraction lines collected during electron backscatter diffraction analysis. We compare augite (Wo ~ 33), pigeonite (Wo ~ 13), orthopyroxene (Wo <4), and olivine. In augite (Wo ~ 33), the M2 site is 8-coordinated, while in pigeonite (Wo ~ 13), the site is 6-coordinated. The larger (8-coordinated) M2 site in augite requires structural expansion along the chain direction. The longer chain is enabled by the substitution of the larger Al for Si. The Al³⁺ substitution for Si⁴⁺ causes a charge deficiency that is made up, in part, by the substitution of V⁴⁺ and V³⁺ in the pyroxene M1 site. This rationale does not fully explain the dramatic decrease in $D_V^{\text{orthopyroxene/melt}}$. In monoclinic pyroxenes, the TOT stacking is characterized by + + + + (indicating the direction), a stacking pattern that produces a monoclinic offset. In orthopyroxene, the stacking is + + - -, which produces an orthorhombic structure. The M2 site is located between the reversed TOT units and is highly constrained to 6-coordination and thus cannot contain significant Ca that requires 8-coordination. Because the M2 site in orthopyroxene is small and constrained, it accommodates less Al in the tetrahedral chains and thus less V in the pyroxene M1 site.

Keywords: Vanadium, partitioning, pyroxene, orthopyroxene, augite, pigeonite, EBSD, valence

INTRODUCTION

The studies of Herd et al. (2002), Herd (2003), Wadhwa (2001), and Goodrich et al. (2003) demonstrated that the oxygen fugacity (f_{O_2}) in martian basalts (as determined from martian meteorites) varies up to four log units, spanning the range from the iron wüstite (IW) to quartz-fayalite-magnetite (QFM; equivalent to IW+3.4) buffers and is correlated with geochemical parameters such as LREE/HREE and initial ⁸⁷Sr/⁸⁶Sr. These correlations have been interpreted as indicating the presence of reduced, incompatible-element-depleted and oxidized, incompatible-element-enriched reservoirs that were produced during the early stages of martian differentiation (~4.5 Ga) (Herd et al. 2002; Herd 2003; Wadhwa 2001; Goodrich et al. 2003; Shih et al. 1982; Borg et al. 1997; Jones 2003). Martian basaltic magmatism, as it is recorded by these martian basalts, is thought to be characterized by mixing between these two reservoirs. Early studies estimated f_{O_2} by two independent approaches, f_{O_2} from mineral equilibria (Herd et al. 2002; Herd 2003; Goodrich et al. 2003) or multivalent behavior of Eu in phases such as pyroxene (Wadhwa 2001). The work of Shearer et al. (2006) used a different approach to evaluate

the f_{O_2} of potential reservoirs that occur in the martian mantle. In that paper, we used the estimated V content of the near-primary martian basalt melt Yamato 980459 (Y98) along with that of one of the earliest phases to crystallize from this basalt (olivine). More recent work by Papike et al. (2013), discusses various V oxybarometers and their applicability.

Our previous studies concerning valence state partitioning of Cr, V, and Eu in pyroxene include several papers on analog QUE 94201 compositions (Karner et al. 2007a, 2007b, 2008, 2010; Papike et al. 2010). This study will compare the results of Papike et al. (2010) and Karner et al. (2010) with the new data collected in this paper. Although other studies have been completed, only these two have f_{O_2} ranges between IW-1 and QFM. Papike et al. (2013) examined V partitioning among olivine, spinel, and melt at f_{O_2} values of IW-1, IW, IW+1, IW+2, and QFM. Both the QUE 94201 analog study (Karner et al. 2010) and the Y98 analog study (Papike et al. 2013) use starting materials spiked with REE, V, and Sc. The QUE 94201 meteorite represents a pyroxene-phyric martian melt and Y98 represents an olivine-phyric martian melt. Therefore the compositions of the host basalts are significantly different and also the crystal structures (augite in QUE 94201, and low-Ca pyroxene in Y98) are quite different. Here, we will address the effect of melt composition and crystal structure on

* E-mail: pvburger@unm.edu

the partitioning of V between pyroxene and melt and use crystal chemical arguments (e.g., Papike et al. 2005) to explain the lower $D_V^{\text{pyroxene/melt}}$ for low-Ca pyroxene vs. augite.

EXPERIMENTAL APPROACH

Experiments were prepared in vertical tube, Deltech gas mixing furnaces at the Johnson Space Center. These runs were made using a spiked composition of martian meteorite Y98. The REEs were added as 0.6 wt% of their oxides (Ce as CeO₂). Sc and V were added as Sc₂O₃ and V₂O₅ and doped to 0.1 wt%. Experimental charges of the Y98 composition were pasted onto Re-wire loops at imposed f_{O_2} values of IW-1, IW, IW+1, IW+2, and QFM. All experiments were held for 8 h at 1500 °C to ensure homogeneity and f_{O_2} equilibration. Charges were then cooled at 1000 °C/h to 1400, 1300, and 1200 °C, and held at the final temperature for at least 48 h, then drop-quenched into water. For experiments conducted at QFM, pressed pellet charges of Y98 were placed onto Pt₆₀Rh₁₀ loops and then air-quenched at the end of the same thermal history as the other f_{O_2} experiments. The Pt-wire loop does not oxidize at high f_{O_2} , whereas the Re-wire loop prevents Fe loss at low f_{O_2} . Analyses of the run products from the 1200 °C experimental phases are presented in Table 1. The 1200 °C temperature was used because we found that for our bulk composition, this is the optimal temperature to have spinel, olivine, pyroxene, and melt in equilibrium. Only three of the five runs contained orthopyroxene rather than pigeonite. They are the runs at IW-1, IW, and QFM. These runs will be emphasized in this paper. These experiments were initially introduced in Papike et al. (2013), where partitioning of V was examined in olivine and spinel.

ANALYTICAL APPROACH

Electron microprobe (EPMA)

Analyses were collected on the JEOL JXA 8200 electron microprobe at the Institute of Meteoritics (IOM) and Department of Earth and Planetary Sciences (E&PS), at the University of New Mexico (UNM). Initial steps included WDS mapping for selected elements in each of the five experiments included in this study. Electron microprobe analyses initially examined the major/minor element chemistry of the experiments and phases of interest (pyroxene and glass). Samples were analyzed under a 15 kV accelerating voltage, 20 nA beam current, and a 2 μm spot for pyroxene and 10 μm for glass. Elements were calibrated using C.M. Taylor Co. EPMA standards, as well as additional standards developed in-house. Measurements consisted of extended peak and background counting times for V in pyroxene, along with the concurrent measurement of Ti concentration. By increasing the counting statistics for both V and Ti (with the

TiKβ peak representing a known interference for VKα), the 3σ detection limit for each was reduced drastically (62 and 95 ppm for V and Ti, respectively). Ferric Fe was calculated using the methodology of Droop (1987). The complete data set for experimental pyroxene and glass at three oxygen fugacities is presented in Table 1 along with the relevant $D_V^{\text{pyroxene/melt}}$ values.

Uncertainties associated with the calculated partition coefficient values (e.g., for $D_V^{\text{pyroxene/glass}}$) were propagated using the 1σ standard deviations and the mean of the EPMA determined vanadium analyses (e.g., Papike et al. 2013). The means and 1σ standard deviations were calculated with a population of >10 spot analyses. Typically, the 1σ standard deviation for a given population of vanadium analyses was greater than the 2σ analytical uncertainty derived from X-ray counting statistics, therefore we feel the use of the 1σ standard deviation is a more accurate portrayal of the actual uncertainties that arise from subtle compositional heterogeneity.

Electron backscatter diffraction (EBSD)

Electron backscatter diffraction is a very useful analytical technique for obtaining structural data in the context of an actual rock. EBSD can only be produced from a highly polished area, and traditional polishing techniques generally leave a “dead layer” at the sample surface, which can lead to poor diffraction patterns. Carbon coating and (ion) beam damage also complicate the collection of a quality pattern. To mitigate these problems, a customized technique was used to prepare the sample. Sample Y98A18 (IW-1), a polished thin section (to 0.3 μm, using alumina paste), was further polished with colloidal silica (0.05 μm) on a Buehler Vibromet at full vibration for 20 min. The sample was imaged and electron backscattered diffraction (EBSD) patterns were generated in the FEI Quanta 3D field emission gun SEM/focused ion beam (FIB) instrument at the University of New Mexico Department of Earth and Planetary Sciences, with the TSL Hikari high-speed EBSD system. Using high-resolution imaging in the FIB, the desired region of the sample was set to the eucentric position. At very high angle (near 70°), an EBSD detector was inserted close to the sample region. With background subtraction turned off, the center of the EBSD was aligned and gain and exposure was minimized. When background subtraction was turned off, a pattern appeared. The best area was chosen and the pattern balance was optimized. Finally, the software assessed the pattern produced, comparing it with theoretical patterns for orthopyroxene and clinopyroxene.

RESULTS AND DISCUSSION

Distinguishing orthopyroxene and pigeonite

Two techniques were used to distinguish orthopyroxene from pigeonite: (1) EPMA traverses and (2) EBSD patterns. The chemical zoning profiles for orthopyroxene have Wo contents <4 mol%, while those for pigeonite have Wo contents >4 mol%. Another chemical characteristic is that Cr decreases with increasing Wo in orthopyroxene, but Cr increases with increasing Wo in pigeonite, which may, at first, seem counter-intuitive. The increasing Cr with increasing Wo in pigeonite occurs because the Ca content of the M2 site causes the site to be eightfold coordinated. This in turn requires two things: (1) for every Cr³⁺ in the M1 (octahedral site), an Al³⁺ is required in the tetrahedral

TABLE 1. Experimental average values

Element (ppm)	IW-1 (Y98A18)	IW (Y98A15)	QFM (Y98A11)
Orthopyroxene			
Al	4051 (473)	3641 (513)	2961 (315)
Mg	158275 (1012)	156849 (1605)	162985 (790)
Ca	13645 (306)	13777 (195)	13411 (312)
Fe ²⁺	113665 (721)	118915 (769)	109314 (717)
Ti	505 (47)	424 (55)	386 (69)
V	993 (94)	862 (131)	500 (54)
Cr	5093 (496)	3755 (497)	2685 (666)
^a Fe ³⁺	10 (34)	131 (416)	188 (703)
Glass			
Al	32242 (380)	31627 (208)	30597 (173)
Mg	57155 (615)	55438 (332)	55638 (524)
Fe ²⁺	141176 (868)	145197 (382)	138829 (496)
Ti	4569 (64)	4577 (64)	4384 (89)
V	917 (64)	891 (64)	1009 (50)
Cr	3531 (39)	2129 (91)	1007 (45)
$D_V^{\text{orthopyroxene/melt}}$	1.08	0.97	0.49

Note: Standard deviation (1σ) shown in parentheses.

^a Estimated using the methodology of Droop (1987).

site for charge balance (Papike et al. 2005) and (2) the larger Ca containing, 8-coordinated site requires a larger tetrahedral chain, which is again aided by Al that is larger than Si in tetrahedral coordination. In orthopyroxene, the Cr³⁺ is charge balanced by a vacancy in the M2 site so that with increasing Wo (Ca in the M2 site), Cr³⁺ decreases because it is unnecessary for charge balance, all else being equal. The EBSD method was discussed in detail above. Nine indexed Kikuchi lines (Miller indices) support the identification of low-Ca pyroxene as orthopyroxene.

Crystal chemical basis for vanadium partitioning behavior in pyroxene

An early demonstration of the effect of the Wo content of pyroxene on *D* values for REE was presented by McKay (1989). He showed that with increasing Wo content, the *D* values for REE increased dramatically, especially for the LREE. McKay states,

“I interpret the partition coefficient variations in terms of the substitution of REE for Ca in the M2 site, and the principle is that the larger the difference between the size of the cation and the site which it will enter, the more incompatible is the cation in that site. The M2 site can accommodate the HREE much more readily than the LREE...”

Papike et al. (2005) lay the foundation for valence state partitioning of Cr, Fe, Ti, Al, and V among crystallographic sites in olivine, pyroxene, and spinel from planetary basalts. This paper illustrated the plethora of possible coupled substitution mechanisms in pyroxene using the following equation (where coefficients indicate the magnitude of the excess/deficiency, such that ^{VI}Al³⁺ is equivalent to 1 charge excess, while 2^{VI}Ti⁴⁺ indicates that for every Ti⁴⁺ substitution, there is a charge excess of 2). The equation expressing this is

$$\begin{aligned} \text{Excesses: } & {}^{\text{VI}}\text{Al}^{3+} + {}^{\text{VI}}\text{Fe}^{3+} + {}^{\text{VI}}\text{Cr}^{3+} + {}^{\text{VI}}\text{V}^{3+} + {}^{\text{VI}}\text{Ti}^{3+} + 2{}^{\text{VI}}\text{Ti}^{4+} + {}^{\text{VI}}2\text{V}^{4+} \\ \text{= Deficiencies: } & {}^{\text{IV}}\text{Al}^{3+} + {}^{\text{M2}}\text{Na}^{+}. \end{aligned}$$

These authors showed the importance of cation size and also charge balance in substitution mechanisms. Figure 1 shows the important effect of Wo content on the vanadium *D* values for pyroxene, with olivine for comparison. Figure 1b shows why V in olivine/melt is a better oxybarometer than V in pyroxene; olivine is not significantly affected by differences in Ca content. Karner et al. (2008) address the V substitution in the pyroxene structure. Coupled substitution is required to incorporate V³⁺ and V⁴⁺ into the pyroxene crystal structure because these cations are replacing divalent Mg and Fe in the M1 site (Papike et al. 2005), thus creating an excess charge of +1 or +2. Crystal charge balance must be maintained and can be accomplished by simultaneously substituting (1) an Al cation(s) into the tetrahedral site for Si or (2) a Na cation(s) into the M2 site for Ca. Both of these substitutions create a charge deficiency of -1 (or -2), and thus neutralize the crystal charge. Therefore, an increase in *D_V* from pigeonite to augite can be explained by the ease with which Al and/or Na can enter augite (compared to pigeonite) for the required charge-balancing coupled substitution. This explanation is supported by Figure 2, which clearly shows that Al and Na increase from

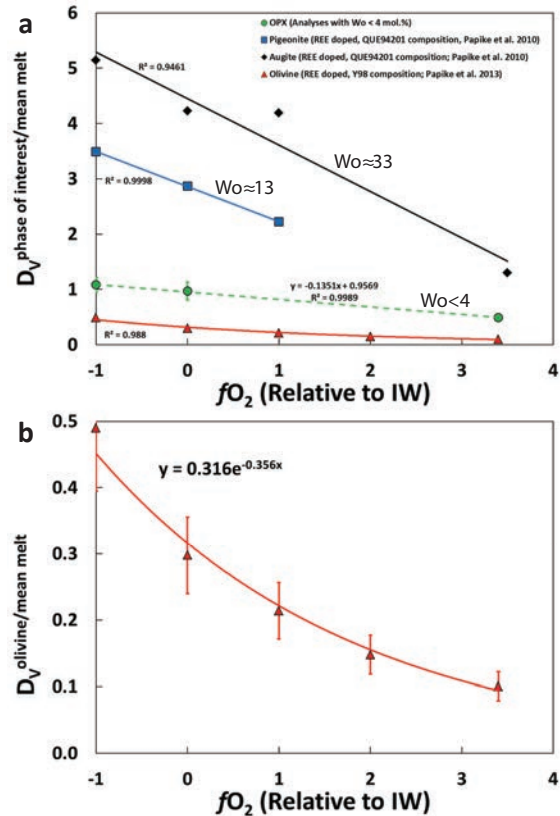


FIGURE 1. (a) *D* values for V in pyroxene/glass for compositions QUE 94201 and Y 980459 (Y98). Results are shown for augite (QUE 94201 composition with Wo = 33 mol%), pigeonite (QUE 94201 composition with Wo = 13 mol%), and orthopyroxene (Y98 composition with Wo <4 mol%). Olivine is also shown for comparison. In all cases, the error bars represent the 1σ propagated error. (b) Olivine *D* values for olivine/melt for comparison.

pigeonite to augite. We emphasize, however, that the Ca content, and structure of augite compared to pigeonite do not sufficiently explain V partitioning into pyroxene. Vanadium partitioning is dependent on both the structure of augite compared to pigeonite, as well as coupled substitution.

While the above discussion explains the difference of *D_V* for augite and pigeonite, it does not explain the much lower *D_V* for orthopyroxene. Papike (1987) shows that there is a very important difference between augite (monoclinic space group *C2/c*) and pigeonite (monoclinic space group *P2₁/c*) versus orthopyroxene (orthorhombic space group *Pbca*), which involves the stacking of tetrahedra-octahedra-tetrahedra (TOT) layers. In monoclinic pyroxenes, the stacking is + + + + (indicates the direction) and this stacking produces the monoclinic offset. In orthopyroxene the stacking is + + - -, which produces an orthorhombic structure. The M2 site is located between the reversed TOT units and is highly constrained to 6-coordination and thus cannot contain significant Ca that requires 8-coordination. Blundy and Wood (1994) provided an excellent model to evaluate the partition coefficient of various elements substituting in the pyroxene crystal structure. Unfortunately, this model does not work very

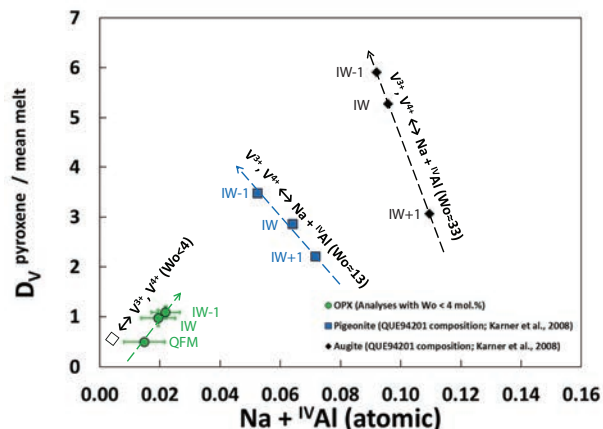


FIGURE 2. Correlations of partition coefficients for V for pyroxene/glass vs. coupled substitution elements, ${}^{\text{IV}}\text{Al}$ and Na. Results are shown for augite (QUE 94201 composition with $W_o = 33$ mol%), pigeonite (QUE 94201 composition with $W_o = 13$ mol%), and orthopyroxene (Y98 composition with $W_o < 4$ mol%). For orthopyroxene, the coupled substitution is V in the M1 site for vacancies in the M2 site. Error bars for orthopyroxene Na + ${}^{\text{IV}}\text{Al}$ values represent the 1σ standard deviation for that parameter. Error bars for $D_V^{\text{pyroxene/melt}}$ as in Figure 1.

well for the M2 site in orthopyroxene because we are dealing with coupled substitution (e.g., V^{4+} in the pyroxene M1 site coupled with 2 Al^{3+} in the pyroxene tetrahedral sites). To apply the Blundy-Wood model, we would have to use two “Onumatype” diagrams, one for 4^+ cations and one for 3^+ cations. The elasticity of the crystal structure site is difficult to determine in such cases. The charge balance exchange is vacancies for V^{3+} , V^{4+} as in olivine (Papike et al. 2005, 2013). That is why orthopyroxene has a different slope (note Fig. 2). For every vacancy, orthopyroxene can accommodate one V^{4+} or two V^{3+} . This is the main reason that V^{3+} is more compatible in the olivine and orthopyroxene structures than V^{4+} .

IMPLICATIONS

This study examines the dramatic increase in $D_V^{\text{pyroxene/melt}}$ with increasing W_o content in pyroxene, and provides an explanation rooted in crystal chemical (atomistic) terms. While this is interesting in general crystal chemistry study of minerals, why is this extremely important for f_{O_2} estimates and martian f_{O_2} studies specifically? The answer is because we have demonstrated that olivine is a more robust oxybarometer as it is not significantly affected by the Ca content, whereas pyroxene is (Papike et al. 2013). In fact Karner et al. (2007a) have stated that valence state partitioning of V and Cr can only be applied as a robust oxybarometer to basalts using experimental data based on the same melt composition and temperature as the unknown.

ACKNOWLEDGMENTS

We acknowledge support for this research from the NASA Cosmochemistry program to Charles Shearer and John Jones.

REFERENCES CITED

- Blundy, J., and Wood, B. (1994) Prediction of crystal–melt partition coefficients from elastic moduli. *Letters to Nature*, 372, 452–454.
- Borg, L.E., Nyquist, L.E., Weismann, H., and Shih, S.-Y. (1997) Constraints on martian differentiation process from Rb–Sr and Sm–Nd isotopic analyses of basaltic shergottite QUE94201. *Geochimica et Cosmochimica Acta*, 61, 4915–4931.
- Droop, G.T.R. (1987) A general equation for estimating Fe^{2+} concentrations in ferromagnesian silicates and oxides from microprobe analyses, using stoichiometric criteria. *Mineralogical Magazine*, 51, 431–435.
- Goodrich, C.A., Herd, C.D.K., and Taylor, L. (2003) Spinel and oxygen fugacity in olivine-phyric and ilherzolithic shergottite. *Meteoritics and Planetary Science*, 38, 1773–1792.
- Herd, C.D.K. (2003) The oxygen fugacity of olivine-phyric martian basalts and the components within the mantle and crust of Mars. *Meteoritics and Planetary Science*, 38, 1793–1805.
- Herd, C.D.K., Borg, L., Jones, J.H., and Papike, J.J. (2002) Oxygen fugacity and geochemical variations in martian basalts: Implications for martian basalt petrogenesis and the oxidation of the upper mantle of Mars. *Geochimica et Cosmochimica Acta*, 66, 2025–2036.
- Jones, J.H. (2003) Constraints on the structure of the martian interior determined from chemical and isotopic signatures of SNC meteorites. *Meteoritics and Planetary Science*, 38, 1807–1814.
- Karner, J.M., Papike, J.J., Shearer, C.K., McKay, G., Le, L., and Burger, P. (2007a) Valence state partitioning between pyroxene–melt: Estimates of oxygen fugacity for martian basalt QUE 94201. *American Mineralogist*, 92, 1238–1241.
- Karner, J.M., Papike, J.J., Sutton, S.R., Shearer, C.K., McKay, G., Le, L., and Burger, P. (2007b) Valence state partitioning of Cr between pyroxene–melt: Effects of pyroxene and melt composition and direct determination of Cr valence states by XANES. *American Mineralogist*, 92, 2002–2005.
- Karner, J.M., Papike, J.J., Sutton, S.R., Shearer, C.K., Burger, P., McKay, G., and Le, L. (2008) Valence state partitioning of V between pyroxene–melt: Effects of pyroxene and melt composition, and direct determination of V valence states by XANES. *Meteoritics and Planetary Science*, 43, 1275–1285.
- Karner, J.M., Papike, J.J., Sutton, S.R., Burger, P.V., Shearer, C.K., Le, L., Newville, M., and Choi, Y. (2010) Partitioning of Eu between augite and a highly spiked martian basalt composition as a function of oxygen fugacity (IW-1 to QFM): Determination of $\text{Eu}^{2+}/\text{Eu}^{3+}$ ratios by XANES. *American Mineralogist*, 95, 410–413.
- McKay, G.A. (1989) Partitioning of rare earth elements between major silicate minerals and basaltic melts. In B.R. Lipin and G.A. McKay, Eds., *Geochemistry and Mineralogy of Rare Earth Elements*, 21, p. 45–77. Reviews in Mineralogy, Mineralogical Society of America, Chantilly, Virginia.
- Papike, J.J. (1987) Chemistry of the rock-forming silicates. Ortho, ring, and single-chain structures. *Reviews in Geophysics*, 25, 1483–1526.
- Papike, J.J., Karner, J.M., and Shearer, C.K. (2005) Comparative planetary mineralogy: Valence state partitioning of Cr, Fe, Ti, and V among crystallographic sites in olivine, pyroxene, and spinel from planetary basalts. *American Mineralogist*, 90, 277–290.
- Papike, J.J., Karner, J.M., Shearer, C.K., and Burger, P.V. (2010) Valence state partitioning of V between augite/melt crystallized from a highly spiked martian basalt composition as a function of oxygen fugacity (IW-1 to FMQ). In *Lunar and Planetary Science* 41, abstract 1010. Lunar and Planetary Institute, Houston.
- Papike, J.J., Burger, P.V., Bell, A.S., Le, L., Shearer, C.K., Sutton, S.R., Jones, J., and Newville, M. (2013) Developing vanadium valence state oxybarometers (spinel–melt, olivine–melt, spinel–olivine) and $V/(\text{Cr} + \text{Al})$ partitioning (spinel–melt) for martian olivine-phyric basalts. *American Mineralogist*, 98, 2193–2196.
- Shearer, C.K., McKay, G., Papike, J.J., and Karner, J.M. (2006) Valence state partitioning of vanadium between olivine–liquid: Estimates of oxygen fugacity of Y980459 and application to other olivine-phyric martian basalts. *American Mineralogist*, 91, 1657–1663.
- Shih, C.-Y., Nyquist, L.E., Bogard, D.D., McKay, G.A., Wooden, J.L., Bansal, B.M., and Weismann, H. (1982) Chronology and petrogenesis of young achondrites, Shergotty, Zagami, and ALHA77005: Late magmatism on a geologically active planet. *Geochimica et Cosmochimica Acta*, 46, 2323–2344.
- Wadhwa, M. (2001) Redox state of Mars’ upper mantle from Eu anomalies in shergottite pyroxene. *Science*, 292, 1527–1530.

MANUSCRIPT RECEIVED OCTOBER 29, 2013

MANUSCRIPT ACCEPTED DECEMBER 31, 2013

MANUSCRIPT HANDLED BY IAN SWAINSON